Regulation of myonuclear positioning and muscle function by the skeletal muscle-specific CIP protein

Jianming Liu[a,1,2], Zhan-Peng Huang[a,b,2], Mao Nie[a,c], Gang Wang[a], William J. Silva[a,d], Qiumei Yang[a,e], Paula P. Freire[a,f], Xiaoyun Hu[a], Huaqun Chen[a,g], Zhongliang Deng[c], William T. Pu[a,h], and Da-Zhi Wang[a,h,3]

[a]Department of Cardiology, Boston Children's Hospital, Harvard Medical School, Boston, MA 02115; [b]Center for Translational Medicine, National Health Commission (NHC) Key Laboratory of Assisted Circulation, The First Affiliated Hospital, Sun Yat-sen University, Guangzhou, 510275, China; [c]Department of Orthopaedic Surgery, The Second Affiliated Hospital, Chongqing Medical University, Chongqing, 400010, China; [d]Laboratório de Biologia Celular e Molecular do Músculo Estriado, University of São Paulo, CEP 05508-000 Cidade Universitária, São Paulo, Brazil; [e]Department of Animal Sciences, Sichuan Agriculture University, Chengdu, 611130, China; [f]Department of Morphology, Institute of Biosciences, São Paulo State University, CEP 18618-000, Botucatu, São Paulo, Brazil; [g]Department of Biology, Nanjing Normal University, Nanjing, 225300, China; and [h]Harvard Stem Cell Institute, Harvard University, Cambridge, MA 02138

Edited by Eric N. Olson, University of Texas Southwestern Medical Center, Dallas, TX, and approved June 17, 2020 (received for review December 31, 2019)

The appropriate arrangement of myonuclei within skeletal muscle myofibers is of critical importance for normal muscle function, and improper myonuclear localization has been linked to a variety of skeletal muscle diseases, such as centronuclear myopathy and muscular dystrophies. However, the molecules that govern myonuclear positioning remain elusive. Here, we report that skeletal muscle-specific CIP (sk-CIP) is a regulator of nuclear positioning. Genetic deletion of sk-CIP in mice results in misalignment of myonuclei along the myofibers and at specialized structures such as neuromuscular junctions (NMJs) and myotendinous junctions (MTJs) in vivo, impairing myonuclear positioning after muscle regeneration, leading to severe muscle dystrophy in *mdx* mice, a mouse model of Duchenne muscular dystrophy. sk-CIP is localized to the centrosome in myoblasts and relocates to the outer nuclear envelope in myotubes upon differentiation. Mechanistically, we found that sk-CIP interacts with the Linker of Nucleoskeleton and Cytoskeleton (LINC) complex and the centriole Microtubule Organizing Center (MTOC) proteins to coordinately modulate myonuclear positioning and alignment. These findings indicate that sk-CIP may function as a muscle-specific anchoring protein to regulate nuclear position in multinucleated muscle cells.

skeletal muscle | nuclear positioning | sk-CIP protein | LINC complex | MTOC

The fusion of skeletal myoblasts to form functional myofibers with well-organized organelles is a complex and highly controlled process (1). However, the molecular mechanisms that control myonuclei arrangement in skeletal muscle remain incompletely understood, and no muscle-specific protein that directly regulates this process has been identified in mammals. The position and movement of a myonucleus can be driven by the cytoskeletal network of microtubules, actin, and/or intermediate filaments (2, 3). While previous studies have implicated the Linker of Nucleoskeleton and Cytoskeleton (LINC) complex in myonuclear positioning, and several mutations in LINC complex proteins indeed cause different skeletal muscle diseases in humans, the precise role of this complex in nuclear movement and positioning during muscle differentiation is still unclear (4–11). Both LINC and the Microtubule Organizing Center (MTOC) are integral parts of the nuclear-cytoskeletal linkages that anchor the microtubule network within the vicinity of the nucleus. More recently, several proteins involved in organizing either the LINC or MTOC complexes have been implicated in regulating myonuclear position and movement during myotube formation (2, 12–17); however, none of these are muscle specific, nor do they appear to be sufficient for complete control of myonuclear distribution along myofibers, suggesting that muscle-specific proteins or additional redundant regulators of this process remain to be discovered. Here, we describe a muscle-specific protein called skeletal muscle CIP (sk-CIP) that plays an important role for proper myonuclear position/alignment within myofibers. sk-CIP mediates the connection between the LINC complex and the microtubule cytoskeleton by participating in the redistribution of MTOC complexes surrounding each myonucleus during muscle differentiation. Loss of CIP in *mdx* mice, an animal model of Duchenne muscular dystrophy (DMD), leads to profound myonuclear positioning defects and severe muscular dystrophy.

Results

CIP Regulates Myonuclear Position during Myogenic Differentiation. We and others have previously identified the CIP gene (Cardiac Islet-1 Interaction Protein), also called Mlip (18, 19), and reported that CIP participates in the regulation of cardiac function in response to stress (20). The CIP gene encodes multiple splicing isoforms, and we discovered an alternatively spliced isoform in skeletal muscle, which we named skeletal muscle CIP (sk-CIP) (Fig. 1*A* and *SI Appendix*, Fig. S1*A*). The CIP sequence

Significance

The arrangement of nuclei in myofibers, which are multinucleated skeletal muscle cells, is essential for their proper function. Abnormal nuclear positioning in myofibers is a common feature of several skeletal muscle diseases, including centronuclear myopathy and muscular dystrophy. Here, we show an isoform of the CIP protein (sk-CIP) contributes to the regulation of the positioning of nuclei in myofibers by interacting with both the LINC complex (Linker of Nucleoskeleton and Cytoskeleton) and proteins in the microtubule-organizing center (MTOC). Through these interactions, sk-CIP appears to function as a skeletal muscle-specific anchoring protein that regulates nuclear positioning in myofibers. Further investigation and understanding of myofiber nuclear positioning may facilitate the development of novel therapies for some diseases of skeletal muscle.

Author contributions: J.L., Z.-P.H., W.T.P., and D.-Z.W. designed research; J.L., Z.-P.H., M.N., G.W., W.J.S., Q.Y., P.P.F., X.H., H.C., Z.D., W.T.P., and D.-Z.W. performed research; J.L., Z.-P.H., M.N., G.W., W.J.S., Q.Y., P.P.F., X.H., H.C., Z.D., W.T.P., and D.-Z.W. analyzed data; and J.L., Z.-P.H., and D.-Z.W. wrote the paper.

The authors declare no competing interest.

This article is a PNAS Direct Submission.

[1]Present address: Vertex Cell and Genetic Therapies (VCGT), Vertex Pharmaceuticals, Watertown, MA 02472.

[2]J.L. and Z.-P.H. contributed equally to this work.

[3]To whom correspondence may be addressed. Email: Da-Zhi.Wang@childrens.harvard.edu.

This article contains supporting information online at https://www.pnas.org/lookup/suppl/doi:10.1073/pnas.1922911117/-/DCSupplemental.

First published July 27, 2020.

is highly conserved among mammals. A search of the Genotype-Tissue Expression (GTEx) Consortium Database reveals that the human homolog of the mouse CIP gene is highly expressed in the heart and skeletal muscle (Fig. 1*B*). A close examination of the distribution of cardiac and skeletal muscle-specific CIP isoforms from the ENCODE database (Fig. 1*C*) and the GTEx Consortium Database (Fig. 1*D*) indicates the existence of cardiac- and skeletal muscle-enriched isoforms in both mouse and human. Interestingly, during C2C12 myoblast differentiation, the expression levels of both sk-CIP and total CIP transcripts are increased, similar to that of myogenin (*SI Appendix*, Fig. S1*B*). We detected increased expression of sk-CIP protein during C2C12 differentiation (*SI Appendix*, Fig. S1*C*). Furthermore, ChIP-Sequencing (ChIP-Seq) data from ENCODE show strong binding of MyoD and myogenin to the CIP gene promoter, indicating that sk-CIP muscle-specific expression is regulated by myogenic transcription factors during myogenic differentiation (*SI Appendix* and Fig. 1*A*).

To begin to assess the function of CIP in skeletal muscle, we first knocked down CIP using a pool of siRNAs in C2C12 cells. Interestingly, we found that inhibition of CIP resulted in nuclear clustering within single myotubes (Fig. 1*E*, arrows, Fig. 1*F*), without affecting myogenic differentiation gene expression (*SI Appendix*, Fig. S1*D*). To further confirm that CIP affects myonuclear positioning, we utilized CRISPR-Cas9 gene editing to create a CIP nonsense mutation to completely abolish CIP expression in C2C12 cells (Fig. 1 *G–I*). Loss of CIP expression is apparent through the loss of multiple bands in Western blots in both siRNA knockdown and CRISPR-Cas9 knockout (KO) experiments, consistent with previous reports of CIP expression (19, 20). CIP knockout in C2C12 myoblasts differentiated into myotubes showed large numbers of nuclei clustered together within single myotubes (Fig. 1 *J* and *K*), confirming the role of sk-CIP in the regulation of myonuclear positioning. Next, we isolated primary myoblasts from the skeletal muscles of CIP knockout mice (19, 20) and subjected them to myogenic differentiation. While wild-type (WT) myoblasts differentiated into long and thin myofibers with well-separated nuclei and efficient spontaneous contraction (Fig. 1 *L* and *M* and Movies S1 and S2), CIP knockout myoblasts differentiated into myotubes containing large numbers of clustered nuclei (Fig. 1 *L* and *M* and *SI Appendix*, Fig. S1*J* and Movies S3–S6). Quantitative analysis confirmed that loss of CIP results in the formation of myonuclear clusters with a significant portion of the CIP mutant myotubes containing more than six aggregated nuclei (Fig. 1*N*). To exclude the possibility that CIP affects myonuclear position indirectly by altering cell proliferation and/or myogenesis, we compared the proliferation and differentiation capacity of WT and CIP-KO myoblasts and found no difference (*SI Appendix*, Fig. S1 *E–I*), suggesting that the myonuclear clustering defect is unlikely to be due to myogenic differentiation defects. Finally, we generated an adenovirus to overexpress sk-CIP, and we found that infecting CIP-KO myoblasts could efficiently rescue the myonuclear clustering defect (Fig. 1*O*), confirming that sk-CIP is responsible for the myonuclear clustering phenotype. Together, these results indicate that CIP is a regulator of nuclear positioning in mammalian skeletal muscle.

Loss of CIP Causes Myonuclear Positioning Defects In Vivo. To test if loss of CIP is indeed affecting skeletal muscle myonuclear positioning in vivo, we turned to CIP-KO mice (19, 20). The CIP-KO mice were generated in a manner such that both cardiac and skeletal muscle isoforms were abolished (19). CIP-KO mice appear to be normal, without gross morphological defects in skeletal muscle, except frequent nuclei cluster at the periphery of myofibers and occasionally internally (Fig. 2*A* and *SI Appendix*, Fig. S2 *A–C*, *J*, and *K*). We did not observe changes in fiber type composition nor sarcolemmal damage (*SI Appendix*, Fig. S2 *D*, *E*, and *H*). Skeletal muscle function appears to be normal in CIP-KO mice despite the frequently observed nuclei clustering around myofibers (*SI Appendix*, Fig. S2 *F* and *G*); however, histological analysis of skeletal muscle from 8-mo-old CIP-KO mice reveals more myonuclear positioning defects in tibialis anterior (TA) muscle (Fig. 2*B* and *SI Appendix*, Fig. S2*I*). The defective myonuclear positioning is manifest even more in later life as various large clusters of nuclei inside individual myofibers are readily detected (*SI Appendix*, Fig. S2*L*). When fractal dimension analysis was applied to binary images to quantify the pattern of myonuclear localization, CIP-KO muscle shows significantly higher complexity of myonuclear positioning than wild-type controls (Fig. 2 *C* and *D*). Analyses and quantification of isolated extensor digitorium longus (EDL) muscle fibers show that most CIP-KO muscle fibers contain more than three myonuclei clustered together (Fig. 2 *E* and *F*). Analysis of the distance between adjacent nuclei in isolated single TA myofibers shows a significant reduction in the subsarcolemma internuclear distance in CIP-KO muscle (*SI Appendix*, Fig. S2 *J* and *K*). The neuromuscular junction (NMJ) is a specialized structure in muscle fibers that mediates the interaction of motor neuron and muscle fiber (21, 22). In wild-type myofibers, NMJs are characterized by acetylcholine receptors (AChRs) surrounding clustered myonuclei within the NMJ region; in contrast, myonuclei at the NMJs fail to be engulfed by AChR clustering and tend to be in contact with each other in CIP-KO muscles (Fig. 2 *G* and *H*). Additionally, at the myotendinous junction (MTJ), where muscle fibers contact tendinous tissues, loss of CIP causes myonuclear rearrangement and clustering, with the clusters sometimes centrally located within the MTJ portion of the myofiber (Fig. 2 *I* and *J*). Collectively, these data demonstrate that sk-CIP plays an important role for proper myonuclear positioning in vivo.

Adult skeletal muscle can regenerate in response to damage, owing to the activation of satellite cells—endogenous myogenic stem cells which proliferate, differentiate, and fuse with residual muscle fibers (23, 24). We tested whether CIP is also involved in myonuclear positioning during muscle regeneration. Skeletal muscle from CIP-KO mice regenerates in a similar pattern as that of control mice after cardiotoxin injection-induced degeneration (*SI Appendix*, Fig. S2*M*), consistent with the view that CIP does not affect the myogenic differentiation program per se; however, there is a profound clustering of centrally localized nuclei (CLN) in regenerated CIP-KO myofibers (Fig. 2*K*). Quantitative analysis reveals a greater number of myofibers containing more than two clustered CLN in CIP-KO muscle (Fig. 2*K*). Therefore, loss of CIP causes myonuclear positioning defects in skeletal muscle fibers during both initial muscle development and adult muscle regeneration.

CIP Is a Component of the LINC Complex and MTOC-Microtubule Cytoskeletal System. To understand the mechanistic action of CIP in the regulation of myonuclear positioning, we first examined the localization of CIP protein in skeletal muscle myoblasts and myotubes. Intriguingly, in contrast to the observation that cardiac CIP protein is predominantly expressed in the cell membrane of cardiomyocytes, we found that sk-CIP predominately colocalizes with γ-tubulin within the centrosome in primary skeletal muscle myoblasts (Fig. 3*A*). In undifferentiated C2C12 myoblasts, sk-CIP protein is found at the perinuclear envelope as well as the centrosome, overlapping with γ-tubulin (Fig. 3*B*). In differentiated C2C12 cells and primary myotubes, sk-CIP protein is predominantly expressed in the cytoplasmic face of the outer nuclear envelope of myonuclei (Fig. 3 *B* and *C*). This dynamic change in sk-CIP localization during myogenic differentiation was also observed when Flag- or EGFP-tagged sk-CIP was overexpressed in both primary myoblasts and C2C12 myoblasts (*SI Appendix*, Fig. S3 *A–E*). We further examined the

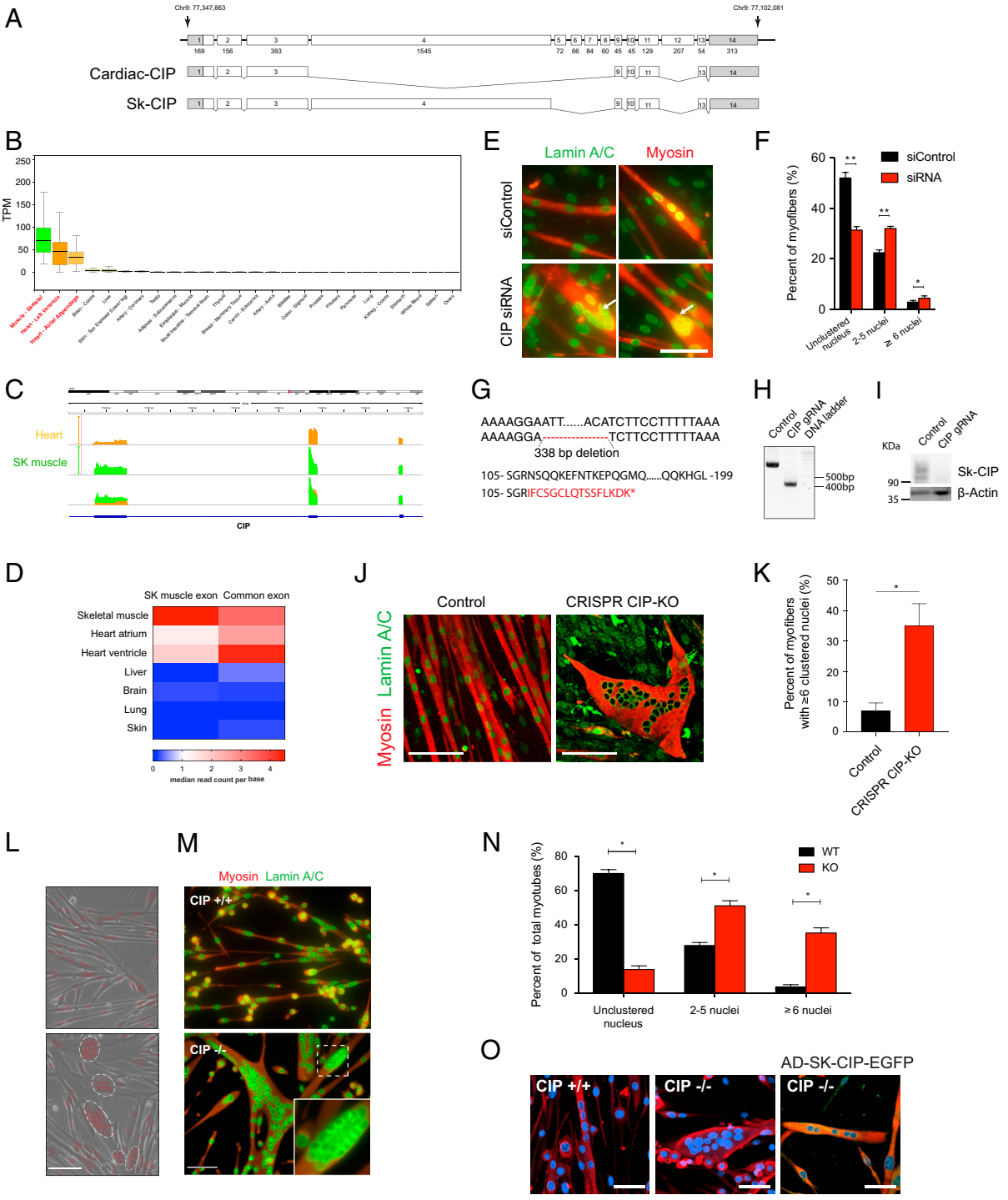

Fig. 1. CIP regulates myonuclear position during myogenic differentiation. (*A*) Schematics for mouse CIP genomic locus as well as cardiac and skeletal muscle mRNA isoforms. The gray box indicates nontranslated sequence and the open box indicates the ORF. (*B*) CIP expression levels across a broad range of human tissues. The graph shows highest CIP expression in striated muscle. Data are derived from the GTEx Consortium. (*C*) RNA-seq signal as density of mapped reads corresponding to muscle-specific exons derived from the ENCODE project. (*D*) Heatmap of skeletal muscle-specific CIP and common CIP expression levels in various tissues. Data are derived from the GTEx Consortium. (*E*) Control and CIP siRNA-infected C2C12 myoblasts differentiated for 5 d and stained with MF20 antibody (myosin) and Lamin A/C. Arrows indicate myonuclear misalignment in myotubes. (Scale bar, 50 μm.) (*F*) Quantification of myonuclei clustering in control and CIP siRNA-treated C2C12 myoblasts. $*P < 0.05$; $**P < 0.001$. (*G*) Diagram of CRISPR-Cas9-mediated knockout of the CIP gene. (*H*) PCR-based genotyping to verify correct targeting of the CIP gene. (*I*) Western blot showing successful knockout of CIP protein. (*J*) Control and CIP knockout C2C12 myoblasts differentiated for 5 d and stained with MF20 antibody (myosin) and Lamin A/C show that CIP is required for myonuclear alignment in myotubes. (Scale bar, 50 μm.) (*K*) Quantification of myonuclear clustering in control and CRISPR-Cas9 CIP-KO C2C12 myoblast cultures ($n = 3$ pairs). $*P < 0.01$. (*L* and *M*) Phase contrast and immunofluorescence images of WT and CIP knockout primary myoblasts differentiated for 2 d and stained with the MF20 antibody (myosin) and Lamin A/C, showing extensive myonuclei clustering in primary CIP-KO myofibers. (Scale bar, 50 μm.) (*N*) Quantification of myonuclei clustering in WT and CIP-KO primary myoblast cultures ($n = 3$ pairs). $*P < 0.001$. (*O*) Infection of primary CIP KO myotubes with sk-CIP EGFP adenovirus resolves nuclear clustering and results in linear alignment of myonuclei.

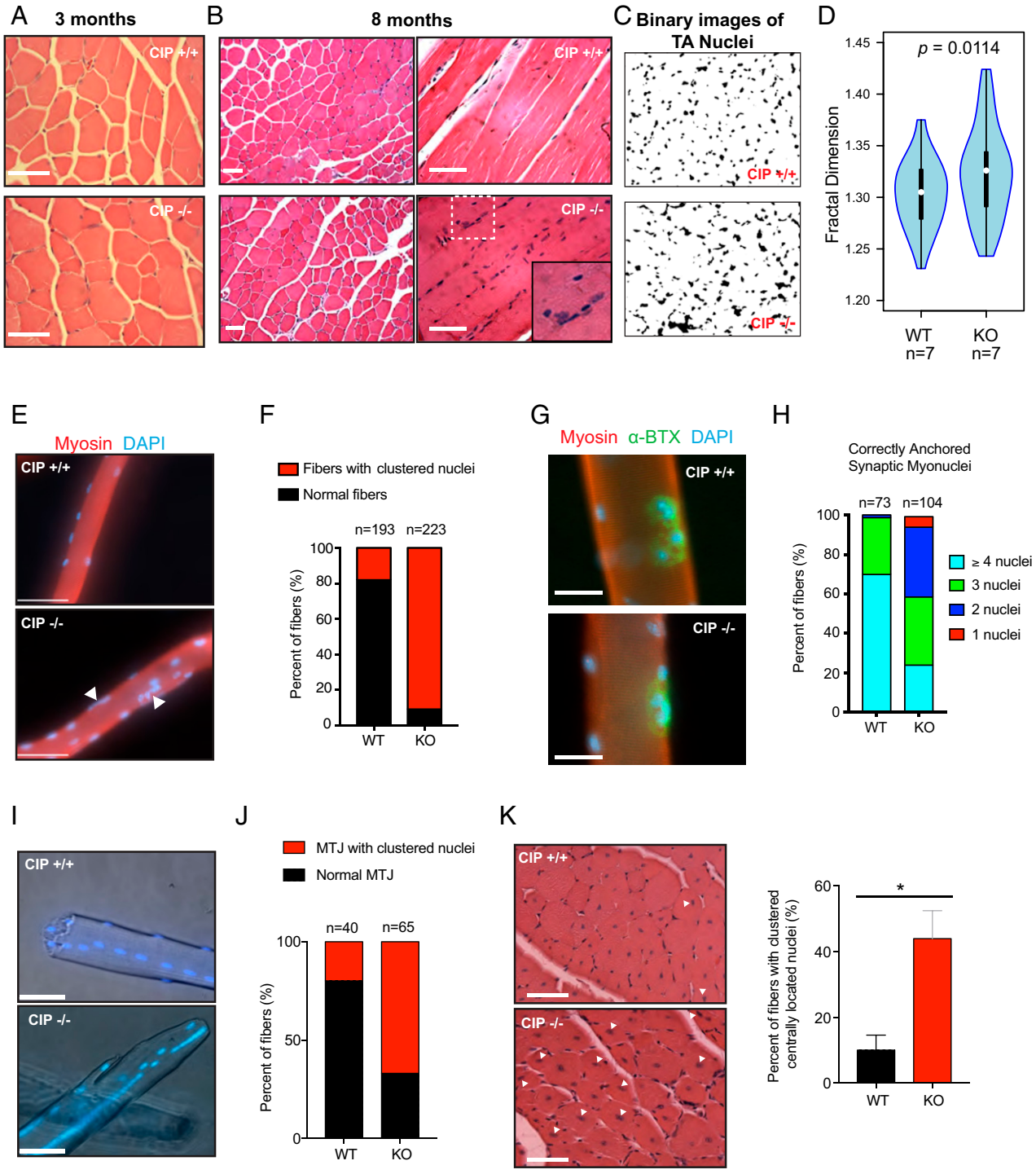

Fig. 2. Loss of CIP causes myonuclear positioning defects in vivo. (*A*) Hematoxylin and Eosin (H&E) staining of cross-sections of 3-mo-old WT and CIP-KO quadricep muscles. (*B*) H&E staining of cross-sections and longitudinal sections of 8-mo-old WT and CIP-KO TA muscles show peripheral myonuclear clustering in CIP-KO myofibers. (*Inset*) Magnified view of the boxed region. (Scale bar, 50 μm.) (*C*) Binary images of nuclear staining of 3-mo-old CIP WT and KO TA muscle. (*D*) Quantification of fractal dimension analysis of WT and KO TA muscle nuclear staining, showing higher disorganization in KO muscles. (*E*) Isolated WT and CIP-KO EDL muscle fibers stained with MF20 (myosin) and DAPI show aberrant myonuclear clustering. (Scale bar, 50 μm.) (*F*) Quantification of myonuclear clustering in WT and CIP-KO isolated EDL muscle fibers shows that most of the CIP-KO muscle fibers contain more than three aggregated myonuclei. n represents the number of muscle fibers. (*G*) Isolated WT and CIP-KO EDL muscle fibers stained with MF20 (myosin), Alexa-488 α-bungarotoxin, and DAPI show aberrant myonuclear anchoring at the neuromuscular junction (NMJ). (Scale bar, 50 μm.) (*H*) Quantification of aberrant myonuclear anchoring at NMJs shows a reduction in the number of myonuclei that are surrounded by AChR in CIP-KO myofibers. (*I*) Isolated WT and CIP-KO EDL muscle fibers stained with DAPI show aberrant myonuclear clustering at the myotendinous junction (MTJ). (Scale bar, 50 μm.) (*J*) Quantification of myonuclear clustering at MTJs in WT and CIP-KO isolated EDL muscle fibers shows significantly more aberrant myonuclear positioning in CIP-KO muscle fibers. (*K*) Cardiotoxin-injured and H&E-stained 3-mo-old TA muscles after 3 wk of regeneration show the aggregation of centrally located myonuclei in CIP-KO mice. (Scale bar, 50 μm.) Arrows indicate clustered, centrally located myonuclei (*Left*). Quantification of aggregated centrally located nuclei in regenerated TA muscle after cardiotoxin injury shows an increase in the percentage of myofibers with aggregated, centrally located nuclei in CIP-KO muscle (*Right*). $n = 4$ animals for each genotype.

in vivo localization of endogenous sk-CIP protein in adult skeletal muscle and found that sk-CIP is localized to the centrosome of satellite cells and the cytoplasmic face of the outer nuclear envelope of myofibers (*SI Appendix*, Fig. S3 *F–I*). Additionally, we detected sk-CIP protein expression underneath the cell membrane of adult skeletal muscle, similar to what is observed in adult cardiomyocytes (*SI Appendix*, Fig. S3 *F–H*). In isolated single myofibers of adult mouse skeletal muscle, sk-CIP protein is also detected outside the outer nuclear envelope (Fig. 3*D* and *SI Appendix*, Fig. S3 *I–K*). Our data therefore reveal dynamic CIP protein localization, from centrosomes in satellite cells to perinuclear outer envelopes in committed myocytes and multinuclear myotubes during myogenic differentiation (Fig. 3 *A–D*).

Next, we tested whether sk-CIP proteins physically interact with components of the MTOC or the LINC complex, the major anchoring protein complex on the nuclear envelope of myonuclei. Using differential detergent extraction and cell fractionation on skeletal muscle from wild-type and CIP-KO mice (serving as a negative control), we found that sk-CIP is associated with mild detergent-resistant cytoskeleton fractions (*SI Appendix*, Fig. S4*A*). sk-CIP is also detected in the nuclear and cytoskeleton fractions of cell lysates that are resistant to mild detergent (*SI Appendix*, Fig. S4 *A–C*), indicating its direct association with the nuclear-cytoskeleton system. Both γ-tubulin and pericentrin are key components of the MTOC complex and are well-characterized centrosome markers. We found that endogenous sk-CIP coimmunoprecipitates with γ-tubulin in skeletal muscle

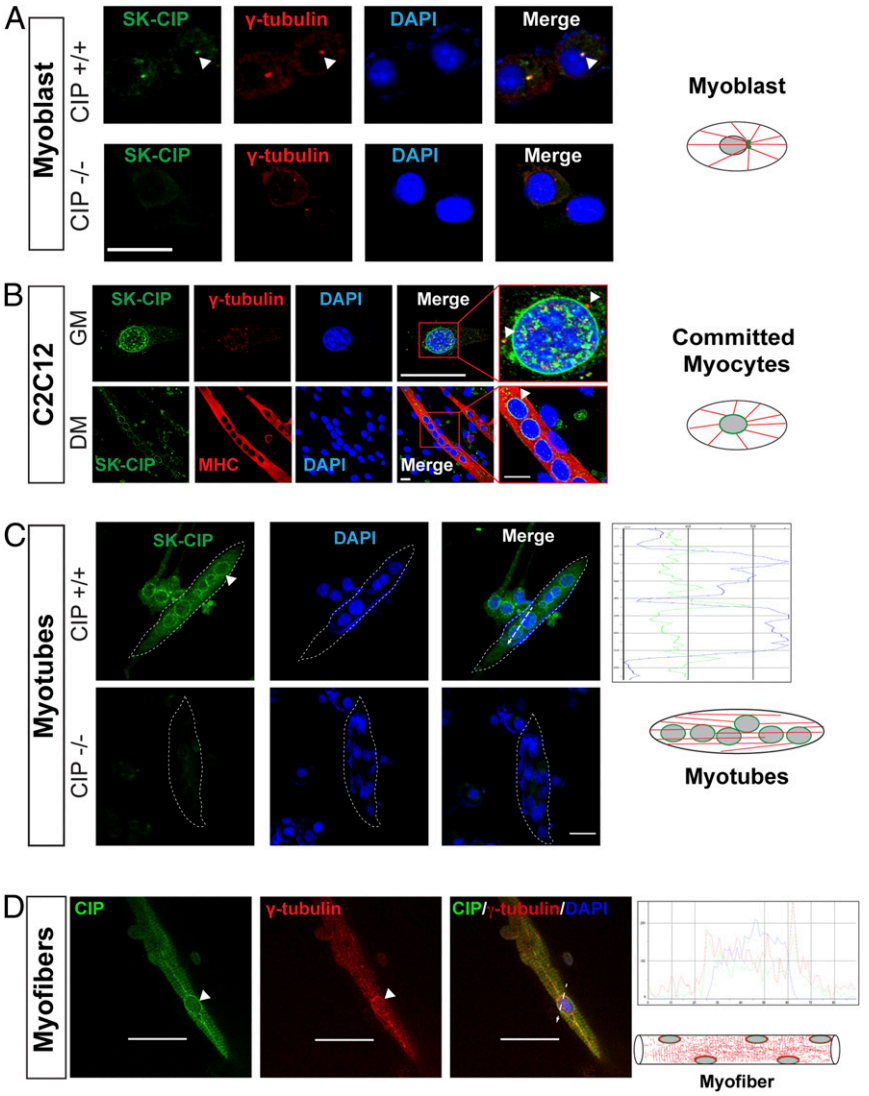

Fig. 3. Skeletal muscle CIP localization changes from the centrosome microtubule organization complex (MTOC) in muscle stem cells to the outer myonuclei membrane ring. (*A*) Confocal images of WT and CIP-KO primary myoblasts stained for CIP (green), γ-tubulin (red), and nuclei (DAPI, blue) show colocalization of CIP and γ-tubulin in the centrosome MTOC. (Scale bar, 20 μm.) The *Right* represents CIP localization in a myoblast (muscle stem cell). (*B*) Confocal images of C2C12 myoblasts and myotubes after a 3-d differentiation stained for CIP (green), γ-tubulin, or myosin, respectively (red), and nuclei (DAPI, blue). A magnified view of the red box is shown to demonstrate the perinuclear localization of CIP relative to the centrosome MTOC complex (arrowhead). (Scale bar, 20 μm.) The *Right* represents CIP localization in committed myocytes. (*C*) Confocal images of WT and CIP-KO primary myoblasts after differentiation for 3 d stained for CIP (green) and nuclei (DAPI, blue) showing redistribution of CIP protein to perimyonuclear ring structures. (Scale bar, 20 μm.) The *Right* represents CIP localization in myotubes. (*D*) Confocal images of an isolated wild-type myofiber stained for CIP (green), γ-tubulin (red), and nuclei (DAPI, blue) showing colocalization of CIP and γ-tubulin around myonuclei. (Scale bar, 50 μm.) Immunofluorescence distribution was quantified for CIP (green line) and γ-tubulin (red line) relative to nuclear (blue line) staining (dashed lines) using Fluoview confocal imaging software. In all schematic diagrams, green represents the CIP protein and red represents the microtubule cytoskeleton in muscle cells.

lysate (Fig. 4*A*). Likewise, Flag-tagged sk-CIP coimmunoprecipitates with pericentrin—a component of the MTOC complex in mammalian cells (Fig. 4*B*). Similarly, we found that sk-CIP interacts with phospho-beta-catenin (Fig. 4*C*), which is another centrosome marker (25, 26).

In addition to MTOC complex proteins, we detected the interaction of sk-CIP with LINC complex proteins, including Sun2, Emerin (Fig. 4 *A* and *D*), and Lamin A/C (*SI Appendix*, Fig. S4 *D* and *E*). Furthermore, we show, using reciprocal immunoprecipitation experiments, sk-CIP directly interacts with SYNE1, another component of the LINC complex (Fig. 4 *E* and *F*). Using fragments of sk-CIP, we found that the middle domain of sk-CIP (encoded by the skeletal muscle-specific exon) is critical for its interaction with Emerin, suggesting that the skeletal muscle-specific isoform of CIP is unique for its nuclear envelope location, essentially linking the nuclear cytoskeleton to regulate myonuclear positioning (Fig. 4 *G* and *H*).

Interestingly, we identified LMO7 as an interacting protein of both cardiac and skeletal muscle CIP isoforms, using both immunoprecipitation and mass spectrometry assays (*SI Appendix*, Fig. S4*E*). We reasoned that loss of CIP could alter the binding preference of nuclear matrix protein Lamin A/C with LMO7, given that LMO7 is a reported transcriptional regulator that shuttles in and out of myonuclei during differentiation (27–29). Indeed, we found that loss of CIP partially disrupted the association of LMO7 with the Lamin A/C, implying the possibility of alteration of the physical properties of myonuclei (*SI Appendix*, Fig. S4*D*). CIP also coimmunoprecipitates β-tubulin and α-actinin, which are structural proteins of the microtubule and actin cytoskeletal systems, respectively. This observation further confirms the association of sk-CIP with muscle cell cytoskeleton structures (*SI Appendix*, Fig. S4*E*). Taken together, our studies reveal that sk-CIP uniquely interacts with components of both LINC and MTOC complexes as well as essential striated muscle cytoskeleton proteins (Fig. 4*I*), suggesting a role in regulating myonuclei dynamics.

Sk-CIP Directly Interacts with LINC and MTOC Complexes to Modulate Myonuclear Positioning. To test whether any of the specific CIP-LINC and CIP-MTOC interactions identified above are required for myonuclear positioning, we generated mutations for genes encoding individual LINC and MTOC components in C2C12 myoblasts or primary myoblasts using CRISPR-Cas9 technology (*SI Appendix*, Fig. S5 *A* and *B*). Interestingly, knockout of LINC proteins SYNE1 and SUN2, results in severe myonuclear positioning defects in C2C12 myoblasts, similar to what we observed in CIP mutant cells (Fig. 5 *A* and *B*). In contrast, loss of SYNE2 and SUN1 does not significantly affect myonuclear positioning (Fig. 5 *A* and *B*), indicating a differential requirement of LINC components. This is consistent with previous reports that show within the LINC complex, there exists functional heterogeneity (4, 5, 7, 16, 30), and that association of SUN1/2 and SYNE1/2 may function in a context-dependent manner. As expected, we found that mutations in both PCM1 and γ-tubulin significantly affect the alignment of myonuclei along C2C12 myotubes (Fig. 5 *A* and *B*). The observed myonuclear clustering defects in these mutant cells appear to be substantially more severe than from loss of CIP (*SI Appendix*, Fig. S5*E*) and are more comparable with that from knockout of MAP7/KIF5b, a recently reported key molecular motor for myonuclear positioning (31). Of particular note, we observed that loss of γ-tubulin also affects myoblast proliferation and differentiation, in a manner where multinuclear syncytial cells fail to differentiate and are myosin negative (*SI Appendix*, Fig. S5*D*, arrows). This is not surprising, given the essential role of γ-tubulin in the formation of the centrosome because this protein has been implicated in regulation of cell division and separation of chromosomes (32, 33). However, mutation of PCNT1, another centrosome protein, did not appear to affect myonuclear positioning (Fig. 5 *A* and *B*), suggesting that only a subset of centrosome proteins work in concert with CIP to regulate myonuclear positioning. Taken together, these results define the function of LINC and MTOC components in regulating myonuclear positioning, highlighting a differential requirement of each member in this process.

To test the genetic and functional interactions between sk-CIP and components of the MTOC and LINC complexes in the regulation of myonuclear positioning, we generated mutations in each of the above LINC and MTOC component genes in CIP-KO primary myoblasts (*SI Appendix*, Fig. S5 *A* and *C*). Knocking out PCNT1 did not exacerbate the myonuclear positioning defects found in CIP-KO myoblasts (Fig. 5*C*). Similar observations were made when SYNE2 or SUN1 were mutated (*SI Appendix*, Fig. S5*F*). In contrast, knockout of SUN2 in CIP-KO myoblasts increases myonuclear clustering when compared with CIP-KO alone (Fig. 5*D*). Disruption of PCM1 or γ-tubulin also exaggerates myonuclear clustering within fused CIP-KO myotubes, further confirming the functional interaction between CIP and the centrosome protein complex (Fig. 5 *E* and *F*). Intriguingly, the CIP/SYNE1 double knockout exhibits strikingly extensive myonuclear clustering within giant myocytes, indicating a synergistic effect between CIP and SYNE1 in regulating myonuclear positioning (Fig. 5*G*). Considering the diverse interaction partners of SYNE1 protein ranging from the actin cytoskeleton and intermediate filaments to the microtubule cytoskeleton (2, 11, 15), part of this synergistic effect may be additive due to other functions of SYNE1 in these processes. Nevertheless, our results highlight the importance of the LINC-CIP-MTOC axis in regulating myonuclei positioning within differentiating myofibers. Loss of a microtubule motor protein or its associated protein, such as Kif5b and MAP, results in a profound myonuclear clustering phenotype in both C2C12 myoblasts and CIP-KO primary myoblasts, consistent with a previous report (31) (*SI Appendix*, Fig. S5*F*). These results establish sk-CIP as a component that bridges the LINC and MTOC complexes to regulate myonuclear positioning in skeletal muscle (Fig. 5*H*).

Loss of CIP and Dystrophin Results in Severe Muscular Dystrophy. Improperly positioned nuclei are hallmarks of numerous muscle disorders, including Duchenne muscular dystrophy and centronuclear myopathies. Patients suffering from many muscle diseases show a varied degree of muscle weakness with incorrectly localized myonuclei. However, it is unclear whether those incorrectly positioned nuclei contribute to the development of the pathology of such muscle diseases. To investigate the pathological impact of CIP-dependent myonuclear positioning defects in muscle diseases, we bred CIP-KO mice with mdx mice, the most commonly used mouse model of Duchenne muscular dystrophy (34). The CIP/*mdx* double knockout mice (DKO) are smaller than age-matched *mdx* mice and show progressive muscular dystrophy as demonstrated by severe kyphosis (Fig. 6 *A* and *B*). DKO mice were unable to fully extend their hind limbs during micro-CT scanning due to skeletal muscle weakness (Fig. 6*B*, arrow). However, loss of CIP did not increase fibrotic and fatty tissue deposits in skeletal muscles; neither did it increase sarcolemmal damage beyond what is found in control *mdx* muscle (Fig. 6 *C* and *D* and *SI Appendix*, Fig. S6 *C–E* and Movie S7). Nevertheless, we observed significantly more clustered central nuclei in the myofibers of DKO mice (Fig. 6 *E* and *F*). When subjected to exercise, DKO mice show dramatically lower activity before and after forced exercise (Fig. 6 *G* and *H*). Most importantly, DKO mice exhibit much weaker skeletal muscle functional output as measured by grip strength (Fig. 6*I*). Together, these data demonstrate that CIP plays an important role in myonuclear positioning during normal skeletal muscle homeostasis and may be one of the contributors to abnormal myonuclear positioning in muscular dystrophy.

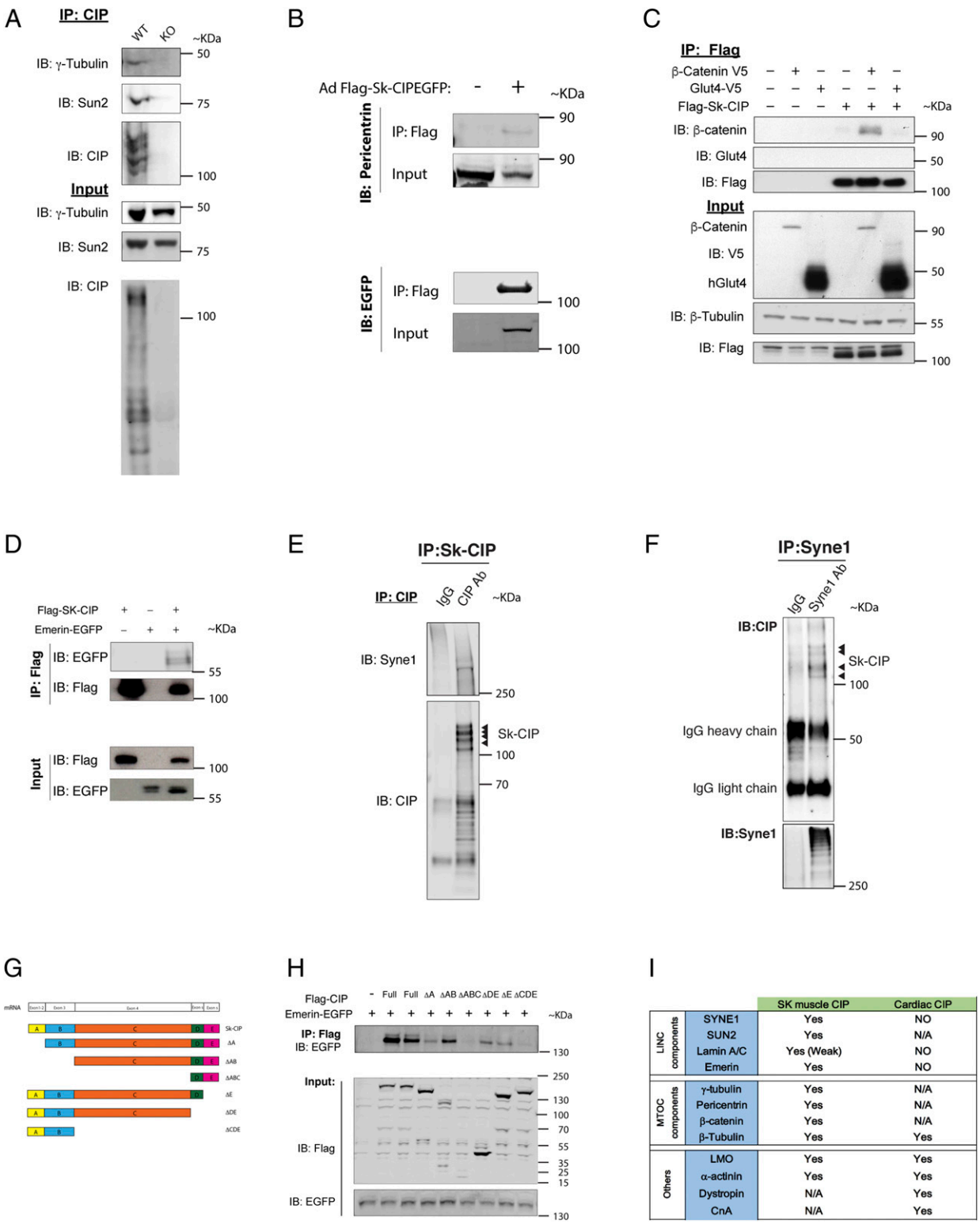

Fig. 4. Skeletal muscle CIP directly interacts with MTOC and LINC complex components. (*A*) Coimmunoprecipitation assays using WT and CIP-KO gastrocnemius muscle protein lysates. (*B*) Coimmunoprecipitation assays using C2C12 myoblasts infected with adenovirus expressing Flag-tagged sk-CIP-EGFP. A pericentrin (PCNT1) antibody was used to detect endogenous pericentrin protein. (*C*) Coimmunoprecipitation assays using HEK293T cells transfected with Flag-tagged sk-CIP and/or V5-tagged β-catenin. A membrane-bound protein, V5-tagged GLUT4, served as a negative interaction control. (*D*) Coimmunoprecipitation assays using HEK293T transfected with Flag-sk-CIP and/or Emerin-EGFP. (*E* and *F*) Immunoprecipitation assays using the indicated antibodies (I, CIP antibody; J, Syne1 antibody) in WT gastrocnemius muscle protein lysates. (*G*) Sk-CIP truncation constructs, FLAG tagged at amino terminals. Letters indicate the protein portion deleted according to mRNA (*Top*) exon numbers (white box). (*H*) Coimmunoprecipitation assays were performed using HEK293T cells transfected with FLAG-tagged sk-CIP truncation constructs and/or Emerin-EGFP. Immunoblotting with EGFP antibody reveals that the long skeletal muscle-specific exon encoded protein fragment is required for CIP ability to link to the LINC complex protein (Emerin). (*I*) Table summarizing skeletal muscle- and cardiac-specific CIP interacting proteins.

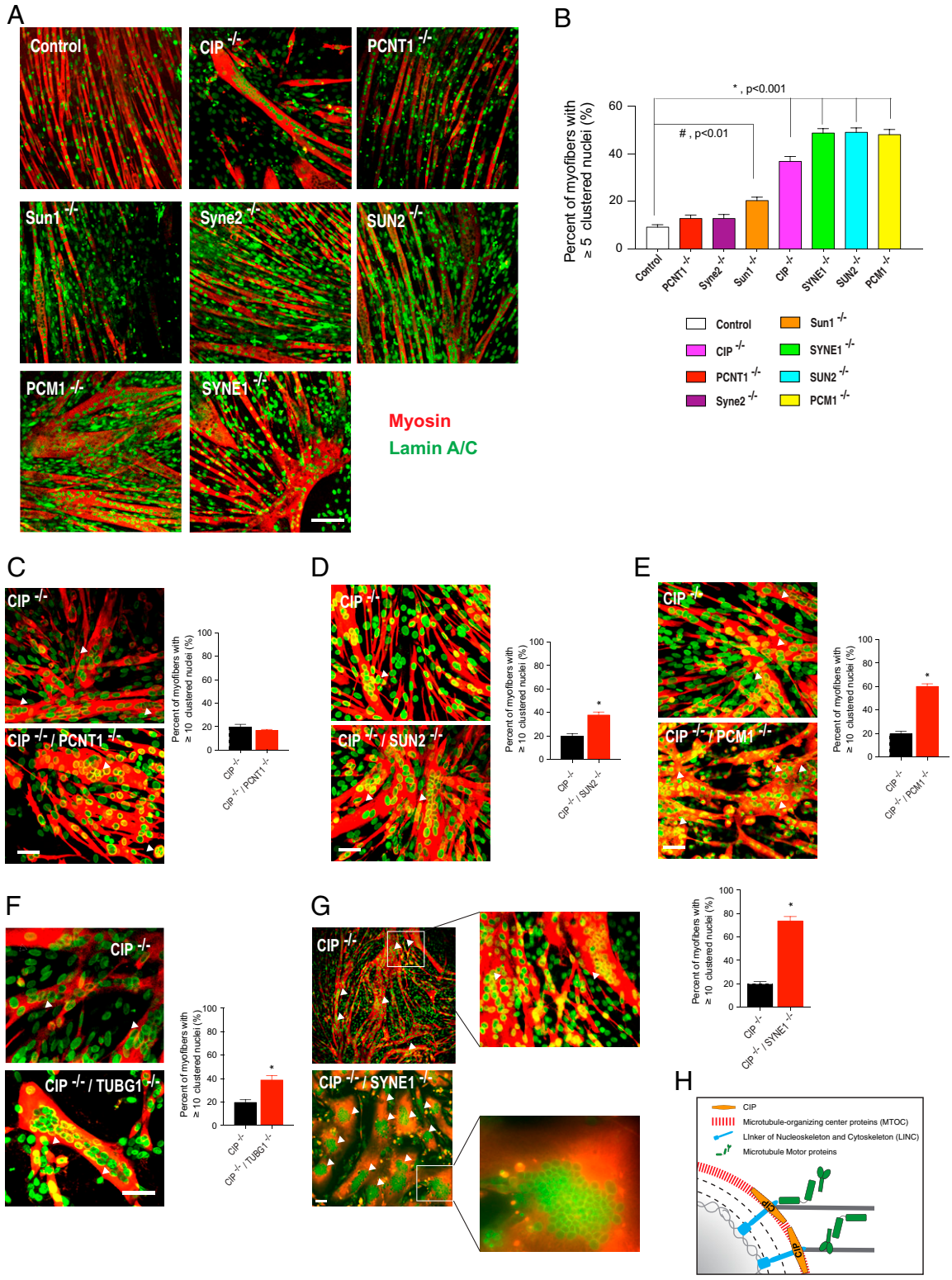

Fig. 5. Skeletal muscle CIP directly bridges MTOC complex proteins with the LINC complex to regulate myonuclear position. (*A*) Representative images of CRISPR-Cas9-mediated LINC or MTOC protein knockout C2C12 myotubes (red for myosin) with nuclei (green for Lamin A/C) clustering. (Scale bar, 100 μm.) (*B*) Quantification of myonuclei clustering (≥5 nuclei) in at least 30 randomly selected microscopic fields in CRISPR-Cas9-mediated LINC or MTOC protein knockout C2C12 myoblasts differentiated for 5 d. Data are from three biological replicates and error bars represent SEM. (*C*–*G*) Immunostaining of MF20 (myosin) (red) and Lamin A/C (green) in CRISPR-Cas9-mediated knockout of each indicated protein in CIP-KO primary myoblasts differentiated for 3 d. (*Insert*) Boxes in *G* are magnified views of the myonuclear aggregation and aberrant localization in CIP knockout and SYNE1/CIP double knockout primary myoblasts differentiated for 3 d. (Scale bar, 50 μm.) Quantification of myofibers containing extensive myonuclei clustering (≥10) in control and CRISPR-Cas9-generated DKO primary myoblast cultures differentiated for 3 d. Error bars indicate SEM. Data are from three independent biological replicates for each cell type. (*H*) Molecular model of sk-CIP function of linking LINC and microtubule cytoskeleton by direct interaction with SYNE proteins and MTOC proteins that are already redistributed to the outer nuclear membrane in mature skeletal muscle fibers.

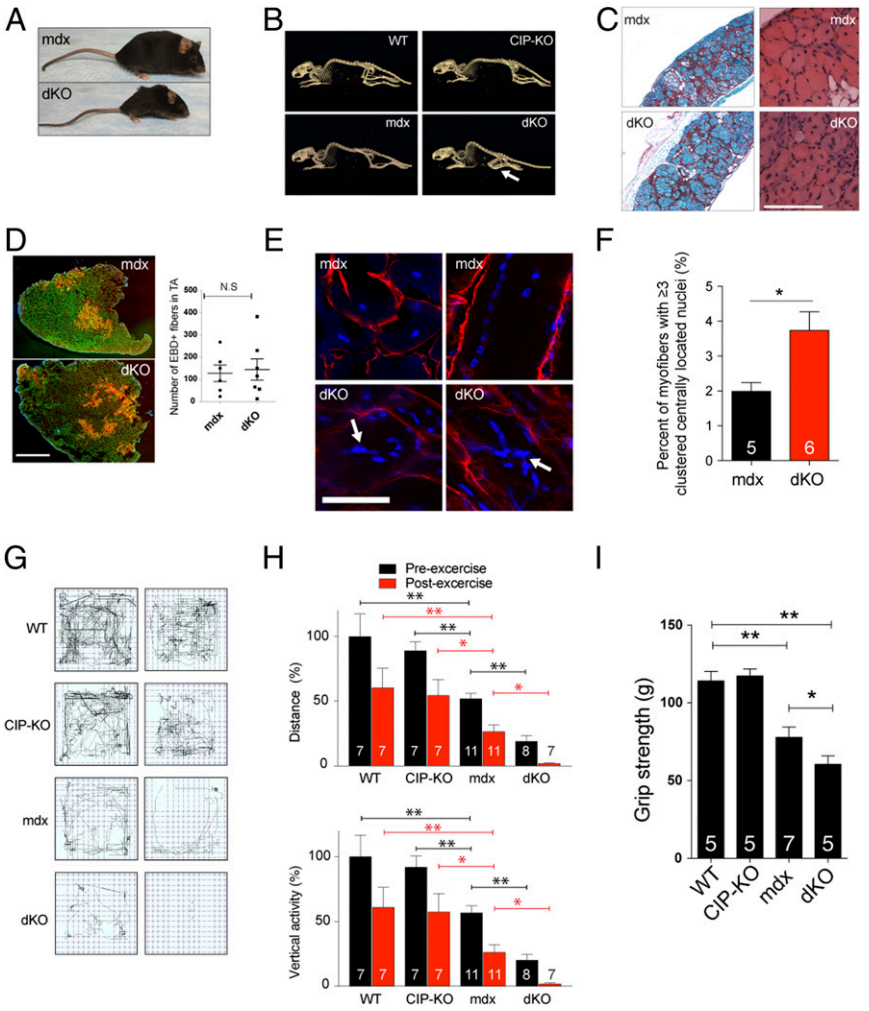

Fig. 6. Loss of CIP and dystrophin results in severe muscular dystrophy. (*A*) Photographs of 1-y-old *mdx* and CIP/*mdx* double knockout mice to illustrate the smaller body size and progressive weakness of DKO mice. (*B*) micro-CT of 1-y-old WT, CIP-KO, *mdx*, and CIP/*mdx* DKO mice showing severe kyphosis in DKO mice. Arrow indicates the inability of DKO mice to fully extend hind limbs due to muscle weakness. (*C*) H&E and Sirius Red/Fast Green staining of diaphragm cross-sections from 1-y-old *mdx* and CIP/*mdx* dKO mice. (Scale bar, 50 μm.) (*D*) Quantification of Evans Blue dye-positive fibers in TA muscles of *mdx* and CIP/*mdx* dKO mice ($n = 6$ for each group). Whole TA muscle stitched images are shown here for representational purposes. (Scale bar, 1 mm.) (*E*) Confocal images of TA muscle stained for laminin to mark myofibers, DAPI to mark nuclei, from 8-wk-old *mdx* and CIP/*mdx* DKO mice. Both cross (*Left*) and longitudinal sectional images (*Right*) reveal a significantly higher degree of disorganized, centrally located myonuclear positioning in DKO mice (arrows). (Scale bar, 50 μm.) (*F*) Quantification of percentage of myofibers with three or more clustered centrally located nuclei in *mdx* and CIP/*mdx* mice, respectively. Animal numbers for each group are indicated on each bar. (*G*) Representative Actitrack activity plots of the four mouse genotypes measured before (preexercise) and after (postexercise) forced downhill treadmill running. The thin line represents the distance traveled, while the dark lines represent instances of rearing (vertical activity). (*H*) Summary graph plotting the total distance and vertical activity of the four genotypes before and after downhill running, respectively. The animal number for each group is indicated under each bar. (*I*) Limb grip strength measurement of mice from the four genotypes, measured in grams. Animal numbers for each group are indicated on each bar.

Discussion

Our studies show sk-CIP is a muscle-specific protein involved in the organization of myonuclear positioning in skeletal muscle cells. We found sk-CIP bridges the LINC and MTOC complexes in skeletal muscle through direct interactions with components of these complexes, and loss of CIP affects myonuclear positioning both in vitro and in vivo (Fig. 5*H* and *SI Appendix*, Fig. S7). Previous studies have suggested that the LINC complex, which spans the nuclear envelope, is important for myonuclear position in both *Drosophila* and mammals (4–9, 11); mutations in several LINC complex proteins, including SYNE1/2, SUN1/2, Emerin, and Lamin A/C, have been linked to various skeletal muscle diseases (4–6, 16, 35). Although it is intuitive that the LINC complex enables the nucleus to interact with the cytoskeleton, and interactions between SYNE proteins and both the microtubule and actin cytoskeleton have been documented, all of these interacting proteins are ubiquitously expressed in all cell types, raising the question of how specificity is established for nuclear movement and positioning in multinucleated muscle cells. Our studies identify CIP as a striated muscle-specific protein that could mediate such a connection specifically in skeletal muscle. Intriguingly, it has been long known that centrosome and pericentriolar proteins, such as γ-tubulin, pericentrin, and PCM1, disperse into the outer nuclear envelope during muscle differentiation (12–14, 17); yet, the molecular and cellular mechanism of this process remains virtually unknown. To our knowledge, sk-CIP is an identified muscle-specific protein that changes its location from centrosome to the myonuclear outer membrane after myoblast differentiation. Our results provide evidence that muscle-specific centrosome proteins directly

participate in the regulation of myonuclear position during myogenic differentiation, and that the previously reported redistribution of centrosome proteins to the outer nuclear envelope in muscle cells may be part of this regulatory process. Of course, additional experiments are needed to establish exactly how CIP interaction with the LINC and MTOC complexes could coordinately regulate nuclear anchoring and movement during muscle differentiation.

Interestingly, our results show that loss of CIP aggravated the dystrophic phenotype in *mdx* mice and resulted in a dramatic reduction in contractile force and overall animal mobility in DKO mice. One simple and straightforward interpretation of this observation is that both dystrophin-dependent myofiber integrity and myonuclear positioning directly contribute to muscle function. Alternatively, we cannot formally exclude the possibility that the phenotype in DKO muscle is due to the loss of small CIP isoforms (cardiac CIP) that can directly interact with dystrophin (Fig. 4*I*), resulting in decreased myofiber cytoskeletal integrity, and that the aberrant myonuclear positioning phenotype is secondary to such defects. However, we think this is unlikely the case because our results from the Evan's Blue dye uptake experiment did not indicate a decrease in membrane integrity in DKO mice (Fig. 6*D*). In addition, although it is likely that the loss of cardiac CIP contributed to the functional phenotype in DKO mice, as revealed through their activity and treadmill running, the lack of additional sarcolemmal damage and clustering of centrally located nuclei to disrupt the sarcomere in DKO mice provides supporting evidence that sk-CIP-regulated myonuclear positioning is, at least, a contributing factor to this severe muscle phenotype. Together, our study suggests that CIP-dependent abnormal myonuclear positioning may further disrupt sarcomeres in *mdx* mice, which could be one of the underlying causes for the decreased function of dystrophic muscle.

Given a recent report associating CIP mutations with cardiomyopathy in human patients (36), we speculate that additional CIP mutations will be linked to skeletal muscle diseases in humans. The discovery of CIP as an essential myonuclear positioning regulator in mammalian skeletal muscle provides an opportunity to better understand this fundamental cellular process. Further investigation and understanding of how dysregulation of myonuclear positioning is associated with different types of muscle defects will facilitate the development of novel therapies for muscle disease.

Materials and Methods

Animals and Animal Procedures. All experimental procedures involving animals in this study were reviewed and approved by the Institutional Animal Care and Use Committee at the Boston Children's Hospital. CIP knockout mice ($CIP^{-/-}$) were generated as previously described (19, 20). Cardiotoxin from *Naja mossambica* (Sigma-Aldrich) was dissolved in sterile saline to a final concentration of 10 μM, divided into aliquots, and stored at −20 °C. Mice were anesthetized with isoflurane according to standard protocols. Mouse legs were shaved and cleaned with alcohol. Tibialis anterior muscles were injected with 50 μL of cardiotoxin solution with a 27-gauge needle. Mouse skeletal muscle tissue for routine histology was harvested and immersion fixed in freshly prepared 4% paraformaldehyde. Subsequent paraffin processing, embedding, sectioning, and H&E staining were performed by standard procedures.

Primary Myoblasts and Single Myofiber Isolation. Primary myoblasts were isolated from neonatal mice as previously described (37). Primary myoblasts were further enriched by preplating 30 min for each passage until near 100% cells were positive for desmin. Primary myoblasts were maintained in Ham's F-10 nutrient mixture-based growth medium containing 20% fetal bovine serum (FBS), 2.5% chicken embryo extract (CEE) (US Biologicals), 5 ng/mL basic fibroblast growth factor (bFGF) (Promega) and 100 U/mL penicillin and 100 μg/mL streptomycin. Differentiation medium DMEM (Dulbecco's modified Eagle medium) with 2% horse serum) was used to induce primary myoblast differentiation.

Single myofibers were isolated from the EDL muscle as previously described (38). For immediate quantification of satellite cells, single fibers were fixed in 4% paraformaldehyde for 10 min at room temperature. Fibers were permeabilized with PBS-T (phosphate-buffered saline [PBS] with 0.5% Triton X-100) for 15 min and blocked with blocking solution (2% bovine serum albumin [BSA]/5% goat serum/0.1% Triton X-100 in PBS) for 1 h at room temperature.

Cell Cultures, Differentiation, and Virus Infection. The 293T cells and C2C12 cells were maintained in 10% FBS with 1% penicillin/streptomycin in DMEM. Primary myoblasts were isolated from wild-type and CIP knockout mouse as previously described (19, 20). Primary myoblasts were maintained in 20% FBS with 1% antibiotic-antimycotic (Thermo Fisher) in F-10 Ham's nutrient mixture (Sigma-Aldrich). For C2C12 and primary myoblasts differentiation, grown media were removed, washed with PBS, and changed into 2% horse serum in DMEM. Fresh differentiation medium was then changed every 2 d after differentiation. Lentivirus expressing CIP-GFP was made as described previously (20). For lentiviral infection, 12 h before infection, cells were seeded in 10-cm dishes at 1×10^6 density and cells were infected for 36 to 48 h before puromycin was added for selection.

Generation of CRISPR sgRNA Knockout Lentivirus and Infection of C2C12 and Primary Myoblasts. Two guide RNAs for each gene targeted to knockout in cell cultures were designed to target the open reading frame (ORF) region close to the translation starting site (*SI Appendix*, Table S1). All guides were individually cloned into the Lenti-CRISPR v2 vector, a gift from Feng Zhang, Broad Institute, MIT, Cambridge, MA (Addgene plasmid No. 52961) (39). For gene-specific sgRNA and control (empty lenti-CRISPR v2) lentivirus production, 5×10^6 Lenti-X 293T cells (Clontech, Cat. No. 632180) were placed in 10-cm tissue culture plates in 10 mL of DMEM containing 10% FBS. Twelve hours later, transfection was performed using Lipofectamine 2000 (Invitrogen) with 13.3 μg lenti-CRISPR v2 plasmid, 7.5 μg psPAX2 plasmid, 5 μg of pMD2.G plasmid. psPAX2 and PMD2.G vectors were gifts from Didier Trono, EPFL, Lausanne, Switzerland (Addgene plasmid Nos. 12260 and 12259). Two days later, lentivirus containing supernatants was filtered through a 0.45-μm filter and concentrated by centrifuging at 22,000 rpm for 2 h in a Ti45 rotor using a Beckman ultracentrifugation machine. Virus pellets were resuspended in 100 μL DMEM. Virus concentrates were aliquoted and store at −80 °C until use.

A portion of freshly made lentivirus was used to measure the titer. Briefly, C2C12 and primary myoblasts were infected with different volumes of viral stock for 2 d, followed by another 2-d selection with puromycin (2 μg/mL). Cell survival was measured and referred to as the infection rate. Based on virus titer, an adjusted amount of virus stock was used to infect C2C12 cells and primary myoblasts for a target multiplicity of infection (MOI) of 5, ensuring that most cells receive at least one lentivirus particle. Two days after transfection, puromycin (Invitrogen) was added to the culture medium at 2 μg/mL to select infected cells for another 3 to 5 d. After selection, cell colonies were cloned and expanded in 24-well plates. A total of 72 to 96 cell clones for each targeted gene were isolated for genomic sequencing confirmation of CRISPR deletion of the target gene. Genomic DNA was purified using a Genomic DNA Purification Kit (Thermo Fisher) according to the manufacturer's instructions. Primers for genotyping PCR are listed in *SI Appendix*, Table S2. PCR products of deletion-positive colonies were gel purified and sequenced to confirm the deletion.

Subcellular Organelle Fractionation. Subcellular protein fractionation was performed with the Subcellular Protein Fractionation Kit for Cultured Cells (Thermo Fisher, No. 78840) according to the manufacturer's instructions. Briefly, myoblasts or myotubes were suspended in ice-cold Dulbecco's phosphate-buffered saline (DPBS) by scraping the surface of the plate with a cell scraper. After centrifuging the cell suspension at $500 \times g$ for 2 min, the cell pellet was washed twice and subjected to a series of subcellular extraction buffers and centrifugation steps to separate each cellular compartment protein lysate. Finally, each protein fraction was mixed with 4× Laemmli sample buffer (Bio-Rad) and analyzed by Western blot.

Immunoprecipitation and Western Blot Analysis. Protein lysates were extracted from cells or tissue using radioimmunoprecipitation assay (RIPA) buffer with 1% Triton X-100 (Boston Bioproducts, BP-116TX) supplemented with Complete protease inhibitor (Sigma-Aldrich) and PhoSTOP phosphatase inhibitor (Sigma-Aldrich) at 4 °C for 15 min. For immunoprecipitation of cytoskeleton structural proteins such as CIP, Syne proteins, and MTOC complexes, lysates were further disrupted mechanically by a brief sonication with a pulse-on time of 5 s and a pulse-off time of 5 s at amplitude of 30 for a total of 200 J

using a microtip sonicator (QSONICA Q700), followed by centrifugation to remove cell debris. Protein concentrations were determined using Bradford assay reagent (Bio-Rad, 5000006) followed by measurement with a FlexStation 3 Microplate Reader (Molecular Devices, Flex3) according to the manufacturer's instructions. Protein samples were mixed with 4× Laemmli sample buffer (Bio-Rad, No. 161-0747) and 20 to 100 μg total protein was loaded and separated on a NuPAGE Bis-Tris Precast gel and transferred to a polyvinylidene fluoride (PVDF) membrane (Millipore), blocked with Odyssey Blocking Buffer (Li-COR) for 1 h at room temperature, and then incubated with the appropriate primary antibody diluted in tris-buffered saline Tween-20 (TBST) with 5% BSA overnight at 4 °C. The horseradish peroxidase (HRP)-conjugated secondary antibody or IRDye dye-conjugated secondary antibody (Li-COR) was diluted in 1:500 or 1:10,000, respectively, in TBST containing 2% BSA. Immunodetection was performed using the Amersham ECL Western Blotting Detection reagent (GE Healthcare) when HRP-conjugated secondary antibodies were used or using the Odyssey CLx imager (Li-COR) when an IRDye dye-conjugated secondary antibody was used.

Quantitative Real-Time PCR. Total RNA was extracted from cultured cells or muscle tissue powered in liquid nitrogen with TRIZOL reagent (Invitrogen) and cDNA was synthesized using iScript Reverse Transcription Supermix (Bio-Rad, 1708841). Gene expression was assessed using standard qPCR approaches with iQ SYBR Green Supermix (Bio-Rad, 1708884). Analysis was performed on a CFX96 Touch Real-Time PCR detection system (Bio-Rad) with the specific primers listed in *SI Appendix*, Table S3. The 2ΔΔCt method was used to analyze the relative changes in gene expression normalized against 60S ribosomal protein L19 (RPL19) expression.

Immunostaining and Histology. Cells were fixed in ice-cold methanol for 5 min in 4 °C and permeabilized with 0.5% Triton X-100 in PBS and blocked with 5% BSA/PBS for 1 h at room temperature. Cells were incubated with primary antibody overnight at 4 °C, followed by incubation with Alexa Fluor-conjugated secondary antibodies (Invitrogen). All antibodies used in this study are listed in *SI Appendix*, Table S4.

For immunostaining of muscle sections, 10 μm optimal cutting temperature compound (OCT)-imbedded frozen sections were fixed with 4% paraformaldehyde for 15 min, permeabilized with 0.1% Triton X-100 for 15 min, and then the section was incubated for 1 h with an M.O.M. blocking kit (Vector Laboratories) to prevent background staining from endogenous mouse immunoglobulins. Sections were subsequently blocked in 10% goat serum prepared with PBS and 0.1% Triton X-100 for 1 h at room temperature. Primary antibodies diluted in PBS containing 2% goat serum and 0.01% Triton X-100 were incubated with sections overnight at 4 °C. Primary antibodies were visualized with Alexa Fluor antibodies (Invitrogen) at a 1:500 dilution for 1 h. Slides were mounted and sealed with VectaShield containing DAPI (Vector Laboratories). Images were acquired on a Nikon Eclipse TE2000 microscope using 20× and 40× objectives or on an Olympus FLUOVIEW FV1000 confocal microscope equipped with an 30× or 60× oil objectives. Images were only adjusted for size without any imaging processing.

Time-Lapse Microscopy. For Movies S1–S7, C2C12 or primary myoblasts were differentiated and time lapse images were visualized using a Nikon Eclipse TE2000 microscope with a chamber for control of temperature and CO_2. Images were captured every hour and then analyzed and assembled using Volocity 5.4.0 software.

Fractal Analysis of Skeletal Muscle Nuclei. To analyze the organization of nuclei by fractal dimension analysis of the TA muscles, photographed slides were binarized by ImageJ (https://imagej.nih.gov/ij/) and the fractal dimension was assessed using box counting. Fractal histological slide analysis was estimated using the relation between the resolution and the scale. The result was quantitatively expressed as the fractal dimension of the object [FD = (Log Nr/log r-1)], where Nr is the number of equal elements needed to cover the original object, and r is the scale applied to the object. Hence, the fractal dimension calculated with ImageJ was expressed from 0 to 2, with values close to 2 representing higher nuclei disorganization.

Quantification and Statistics. Each histological analysis of skeletal muscle was performed on 4 to 6 samples per genotype. For each quantification of in vitro cell differentiation assays at least three independent experiments were performed in duplicate and at least 10 random fields were imaged per sample. Data are presented as mean ± SEM. Differences between groups were tested for statistical significance using one-way ANOVA with Tukey's post hoc multiple comparisons or an unpaired two-tailed Student's *t* test in the case of two-group comparison using Prism 7.0 software, and $P < 0.05$ was considered significant.

Data and Materials Availability. All data needed to evaluate the conclusions in the paper are present in the paper and/or *SI Appendix*.

ACKNOWLEDGMENTS. We thank members of the Da-Zhi Wang laboratory for their discussion and support. We thank Douglas B. Cowan for editing the manuscript. This work is supported by the NIH Grant (HL116919, HL125925) and the Muscular Dystrophy Association Grant (294854, to D.-Z.W.). J.L. is supported by NIH Program T32HL007572 and a Muscular Dystrophy Association Development Grant (186548). Z.-P.H. is supported by the National Natural Science Foundation of China (No. 81873463), Guangdong Science and Technology Department (2018A050506026), and an American Heart Association Scientist Development Grant (16SDG29760000).

1. J. A. Hill, E. N. Olson, *Muscle: Fundamental Biology and Mechanisms of Disease*, (Academic Press, London; Waltham, MA, ed. 1, 2012).
2. E. S. Folker, M. K. Baylies, Nuclear positioning in muscle development and disease. *Front. Physiol.* **4**, 363 (2013).
3. B. Cadot, V. Gache, E. R. Gomes, Moving and positioning the nucleus in skeletal muscle–one step at a time. *Nucleus* **6**, 373–381 (2015).
4. Q. Zhang *et al*., Nesprin-1 and -2 are involved in the pathogenesis of Emery Dreifuss muscular dystrophy and are critical for nuclear envelope integrity. *Hum. Mol. Genet.* **16**, 2816–2833 (2007).
5. K. Lei *et al*., SUN1 and SUN2 play critical but partially redundant roles in anchoring nuclei in skeletal muscle cells in mice. *Proc. Natl. Acad. Sci. U.S.A.* **106**, 10207–10212 (2009).
6. M. J. Puckelwartz *et al*., Disruption of nesprin-1 produces an Emery Dreifuss muscular dystrophy-like phenotype in mice. *Hum. Mol. Genet.* **18**, 607–620 (2009).
7. X. Zhang *et al*., SUN1/2 and Syne/Nesprin-1/2 complexes connect centrosome to the nucleus during neurogenesis and neuronal migration in mice. *Neuron* **64**, 173–187 (2009).
8. M. J. Puckelwartz *et al*., Nesprin-1 mutations in human and murine cardiomyopathy. *J. Mol. Cell. Cardiol.* **48**, 600–608 (2010).
9. E. Mattioli *et al*., Prelamin A-mediated recruitment of SUN1 to the nuclear envelope directs nuclear positioning in human muscle. *Cell Death Differ.* **18**, 1305–1315 (2011).
10. I. Banerjee *et al*., Targeted ablation of nesprin 1 and nesprin 2 from murine myocardium results in cardiomyopathy, altered nuclear morphology and inhibition of the biomechanical gene response. *PLoS Genet.* **10**, e1004114 (2014).
11. M. J. Stroud, I. Banerjee, J. Veevers, J. Chen, Linker of nucleoskeleton and cytoskeleton complex proteins in cardiac structure, function, and disease. *Circ. Res.* **114**, 538–548 (2014).
12. S. J. Doxsey, P. Stein, L. Evans, P. D. Calarco, M. Kirschner, Pericentrin, a highly conserved centrosome protein involved in microtubule organization. *Cell* **76**, 639–650 (1994).
13. M. Bettencourt-Dias, D. M. Glover, Centrosome biogenesis and function: Centrosomics brings new understanding. *Nat. Rev. Mol. Cell Biol.* **8**, 451–463 (2007).
14. V. Srsen, X. Fant, R. Heald, C. Rabouille, A. Merdes, Centrosome proteins form an insoluble perinuclear matrix during muscle cell differentiation. *BMC Cell Biol.* **10**, 28 (2009).
15. D. A. Starr, H. N. Fridolfsson, Interactions between nuclei and the cytoskeleton are mediated by SUN-KASH nuclear-envelope bridges. *Annu. Rev. Cell Dev. Biol.* **26**, 421–444 (2010).
16. P. Meinke *et al*., Muscular dystrophy-associated SUN1 and SUN2 variants disrupt nuclear-cytoskeletal connections and myonuclear organization. *PLoS Genet.* **10**, e1004605 (2014).
17. A. Espigat-Georger, V. Dyachuk, C. Chemin, L. Emorine, A. Merdes, Nuclear alignment in myotubes requires centrosome proteins recruited by nesprin-1. *J. Cell Sci.* **129**, 4227–4237 (2016).
18. E. Ahmady *et al*., Identification of a novel muscle A-type lamin-interacting protein (MLIP). *J. Biol. Chem.* **286**, 19702–19713 (2011).
19. Z.-P. Huang *et al*., CIP, a cardiac Isl1-interacting protein, represses cardiomyocyte hypertrophy. *Circ. Res.* **110**, 818–830 (2012).
20. Z.-P. Huang *et al*., Cardiomyocyte-enriched protein CIP protects against pathophysiological stresses and regulates cardiac homeostasis. *J. Clin. Invest.* **125**, 4122–4134 (2015).
21. R. Rudolf, M. R. Deschenes, M. Sandri, Neuromuscular junction degeneration in muscle wasting. *Curr. Opin. Clin. Nutr. Metab. Care* **19**, 177–181 (2016).
22. L. Li, W. C. Xiong, L. Mei, Neuromuscular junction formation, aging, and disorders. *Annu. Rev. Physiol.* **80**, 159–188 (2018).
23. S. D. Gopinath, T. A. Rando, Stem cell review series: Aging of the skeletal muscle stem cell niche. *Aging Cell* **7**, 590–598 (2008).
24. S. Kuang, M. A. Rudnicki, The emerging biology of satellite cells and their therapeutic potential. *Trends Mol. Med.* **14**, 82–91 (2008).
25. S. Bahmanyar *et al*., beta-Catenin is a Nek2 substrate involved in centrosome separation. *Genes Dev.* **22**, 91–105 (2008).
26. M. V. Hadjihannas, M. Brückner, J. Behrens, Conductin/axin2 and Wnt signalling regulates centrosome cohesion. *EMBO Rep.* **11**, 317–324 (2010).

27. E. Semenova, X. Wang, M. M. Jablonski, J. Levorse, S. M. Tilghman, An engineered 800 kilobase deletion of Uchl3 and Lmo7 on mouse chromosome 14 causes defects in viability, postnatal growth and degeneration of muscle and retina. *Hum. Mol. Genet.* **12**, 1301–1312 (2003).
28. J. M. Holaska, S. Rais-Bahrami, K. L. Wilson, Lmo7 is an emerin-binding protein that regulates the transcription of emerin and many other muscle-relevant genes. *Hum. Mol. Genet.* **15**, 3459–3472 (2006).
29. Z. Dedeic, M. Cetera, T. V. Cohen, J. M. Holaska, Emerin inhibits Lmo7 binding to the Pax3 and MyoD promoters and expression of myoblast proliferation genes. *J. Cell Sci.* **124**, 1691–1702 (2011).
30. K. J. Roux *et al*., Nesprin 4 is an outer nuclear membrane protein that can induce kinesin-mediated cell polarization. *Proc. Natl. Acad. Sci. U.S.A.* **106**, 2194–2199 (2009).
31. T. Metzger *et al*., MAP and kinesin-dependent nuclear positioning is required for skeletal muscle function. *Nature* **484**, 120–124 (2012).
32. J. M. Kollman, A. Merdes, L. Mourey, D. A. Agard, Microtubule nucleation by γ-tubulin complexes. *Nat. Rev. Mol. Cell Biol.* **12**, 709–721 (2011).
33. A. D. Sanchez, J. L. Feldman, Microtubule-organizing centers: From the centrosome to non-centrosomal sites. *Curr. Opin. Cell Biol.* **44**, 93–101 (2017).
34. G. Bulfield, W. G. Siller, P. A. Wight, K. J. Moore, X chromosome-linked muscular dystrophy (mdx) in the mouse. *Proc. Natl. Acad. Sci. U.S.A.* **81**, 1189–1192 (1984).
35. M. Raffaele Di Barletta *et al*., Different mutations in the LMNA gene cause autosomal dominant and autosomal recessive Emery-Dreifuss muscular dystrophy. *Am. J. Hum. Genet.* **66**, 1407–1412 (2000).
36. U. Esslinger *et al*., Exome-wide association study reveals novel susceptibility genes to sporadic dilated cardiomyopathy. *PLoS One* **12**, e0172995 (2017).
37. M. L. Springer, T. A. Rando, H. M. Blau, Gene delivery to muscle. *Curr. Protoc. Hum. Genet.* **Chapter 13**, Unit13.4 (2002).
38. A. Pasut, A. E. Jones, M. A. Rudnicki, Isolation and culture of individual myofibers and their satellite cells from adult skeletal muscle. *J. Vis. Exp.*, e50074 (2013).
39. N. E. Sanjana, O. Shalem, F. Zhang, Improved vectors and genome-wide libraries for CRISPR screening. *Nat. Methods* **11**, 783–784 (2014).